Available online at www.sciencedirect.com
SCIENCE DIRECT
Journal of Magnetic Resonance 179 (2006) 38–48
JMR Journal of Magnetic Resonance
www.elsevier.com/locate/jmr

Symmetry-based recoupling of ^{17}O–^{1}H spin pairs in magic-angle spinning NMR

Jacco D. van Beek [a,1], Ray Dupree [b], Malcolm H. Levitt [a,*]

[a] School of Chemistry, Southampton University, Highfield, Southampton, SO17 1BJ, UK
[b] Department of Physics, University of Warwick, Coventry, CV4 7AL, UK

Received 17 September 2005; revised 31 October 2005
Available online 23 November 2005

Abstract

We have performed magic-angle-spinning solid-state NMR experiments in which protons are recoupled to oxygen-17 nuclei by applying a symmetry-based recoupling sequence at the proton Larmor frequency. Two-dimensional quadrupole-dipole correlation spectra are produced, in which the second-order quadrupolar shift of the oxygen-17 central transition is correlated with the recoupled heteronuclear dipole–dipole interaction. These spectra are sensitive to the relative orientation of the electric field gradient at the site of the oxygen-17 nucleus and the O–H internuclear vector. We also demonstrate experiments in which polarization is transferred from protons to oxygen-17, and show that oxygen-17 signals may be selected according to the protonation state of the oxygen site. We discuss the small observed value of the heteronuclear dipolar splitting in the central-transition oxygen-17 spectra.

Keywords: Solid-state NMR; Quadrupolar nuclei; Oxygen-17; Correlation spectroscopy; Symmetry-based recoupling; MAS; Brucite

1. Introduction

^{17}O solid-state NMR of isotopically enriched materials is an important method for studying a wide range of substances, including zeolites [1–3], glasses [4], battery materials [5], and membrane-bound peptides [6]. The NMR of ^{1}H–^{17}O pairs is of particular interest for the study of acidic sites and hydrogen-bonded systems [3,7,8] since the ^{17}O quadrupole interaction and chemical shift tensors are sensitive to local structural perturbations [9]. Furthermore, the magnitude of the ^{1}H–^{17}O dipole–dipole coupling, and its relative orientation with respect to the chemical shift and quadrupole coupling tensors of the ^{17}O nucleus [10] provide additional information.

The ^{1}H–^{17}O dipole–dipole coupling constant has a magnitude of around 15 kHz in a directly bonded hydroxyl moiety. Although this a considerable interaction, it is difficult to observe, since ^{17}O nuclei in hydroxyl sites experience a large electric field gradient, leading to a second-order quadrupolar broadening of the ^{17}O central transition by several kHz at typical magnetic fields. Furthermore, in many samples, strong ^{1}H–^{1}H interactions create additional complications. Nevertheless, the ^{1}H–^{17}O dipolar coupling has been resolved in static samples by performing Hartmann–Hahn cross-polarization from ^{1}H to ^{17}O, while spin-locking the ^{1}H nuclei by off-resonance irradiation satisfying the Lee-Goldburg condition, in order to reduce the effect of the ^{1}H–^{1}H couplings [10]. Two-dimensional spectroscopy was used to correlate the second-order quadrupolar shift of the ^{17}O central transition with the ^{1}H–^{17}O dipolar coupling, allowing determination of the relative orientation of the ^{1}H–^{17}O dipolar coupling and ^{17}O quadrupolar interaction tensors [10]. In this paper, such two-dimensional spectra are termed quadrupole-dipole (QD) correlation spectra.

It would be desirable to perform QD correlation experiments under magic-angle-spinning (MAS) conditions,

* Corresponding author. Fax: +44 23 8059 3781.
E-mail address: mhl@soton.ac.uk (M.H. Levitt).
[1] Present Address: Physical Chemistry, ETH Zurich, CH-8093 Zurich, Switzerland.

1090-7807/$ - see front matter © 2005 Elsevier Inc. All rights reserved.
doi:10.1016/j.jmr.2005.11.003

since this would allow the ^{1}H–^{17}O dipolar coupling information to be combined with chemical site selectivity, particularly if multiple-quantum magic-angle-spinning (MQMAS) [11,12] or satellite-transition magic-angle-spinning (STMAS) [13,14] are used. Unfortunately, Hartmann–Hahn cross-polarization is problematic for quadrupolar nuclei in the presence of MAS, due to the breakdown of the central-transition spin-lock [15–17]. Alternative schemes, such as those based on REDOR [18–22] or TEDOR [19,23] also have problems, due to the strong homonuclear ^{1}H–^{1}H couplings present in many samples. Here we show that these difficulties may be avoided by using symmetry-based recoupling sequences [24–26]. A suitable choice of recoupling symmetry numbers implements ^{1}H–^{1}H dipolar decoupling at the same time as ^{1}H–^{17}O dipolar recoupling. We demonstrate quadrupole–dipolar (QD) correlation spectroscopy under MAS conditions for two different ^{17}O-labelled molecular systems. The QD correlation spectra have a strikingly different appearance, reflecting their sensitivity to the relative tensor orientations. We also demonstrate significant polarization transfer from the ^{1}H nuclei to the ^{17}O central transition, allowing the ^{17}O spectrum to be edited according to the protonation of the ^{17}O site.

Heteronuclear recoupling leads to splittings in the central-transition ^{17}O spectra. However, the observed splittings are significantly smaller than expected from the OH distance as estimated by neutron diffraction. We discuss various explanations for these discrepancies below but cannot yet provide a definitive explanation.

2. Pulse sequences

Fig. 1 shows two pulse sequences suitable for ^{1}H–^{17}O dipolar recoupling in the presence of MAS. Both methods exploit symmetry-based recoupling sequences of the class RN_n^v applied at the ^{1}H Larmor frequency. The selection rule theorems [24–26] allow one to choose symmetry numbers N, n, and v which implement recoupling of heteronuclear spin interactions, while removing the effect of ^{1}H–^{1}H spin interactions, to first order in average Hamiltonian theory. In all of the experiments described in this paper, we used a recoupling pulse sequence with the symmetry $R18_2^5$, using the simplest possible basic element of a single 180° pulse. The $R18_2^5$ sequence consists of a repetition of the two-pulse element $180_{50}180_{-50}$, where the pulse flip angles and phases are specified in degrees, and the rf field strength corresponds to a nutation frequency of 4.5 times the MAS frequency. This sequence may be shown on symmetry grounds [24–27] to recouple the heteronuclear ^{1}H–^{17}O dipole–dipole interactions whilst decoupling the homonuclear ^{1}H–^{1}H dipolar interactions. Note, however, that the $R18_2^5$ sequence also recouples the ^{1}H chemical shift anisotropy (CSA): in high magnetic fields, the recoupled proton chemical shift anisotropy can interfere with the heteronuclear recoupling performance, as is described below.

In practice the sequence $R18_2^5$ is especially suitable for heteronuclear recoupling experiments at a magic-angle spinning frequency of around 15–20 kHz (requiring rf field strengths of 67.5–90 kHz). Symmetries with different ratios of nutation frequency to spinning frequency are available [24–26]. For example, the sequence $R18_1^7$ was used at 10 kHz MAS frequency, yielding similar results to the ones presented here (not shown).

Fig. 1A shows the PRESTO-II (phase-shifted recoupling effects a smooth transfer of order) [27] pulse sequence. This method has already been used for heteronuclear polarization transfer in spin-1/2 systems. In the first interval, denoted τ_0, a $R18_2^5$ sequence is applied to the Zeeman-polarized ^{1}H nuclei, to decouple the ^{1}H–^{1}H interactions and recouple the ^{1}H–^{17}O interactions. A state of transverse ^{1}H polarization, antiphase with respect to the ^{17}O spin states, is generated at the end of τ_0. A 90° pulse on the ^{17}O central transition is applied, followed by evolution under a second $R18_2^5$ sequence for an interval τ_1. This second $R18_2^5$ sequence has an overall phase shift of 90°, and need not be complete, so that in general it is not equal to an integer number of rotor periods. A 180° pulse is applied to the ^{17}O central transition, and centred around a time point which is T after the end of the ^{17}O 90° pulse. The interval T must be equal to a constant integer number of rotor periods, independent of the value of τ_1. ^{17}O signals are acquired starting from an interval T after the centre of the ^{17}O 180° pulse. The lower half of the PRESTO-II pulse sequence corresponds to a rotor-synchronized Hahn echo applied to the ^{17}O central transition, which refocuses the isotropic ^{17}O chemical shift, the ^{17}O chemical shift anisotropy, and the second-order ^{17}O quadrupolar interaction. TPPM-modulated ^{1}H irradiation [28] is used to suppress heteronuclear interactions during that part of the spin echo which is not occupied by the $R18_2^5$ sequence, and during signal acquisition.

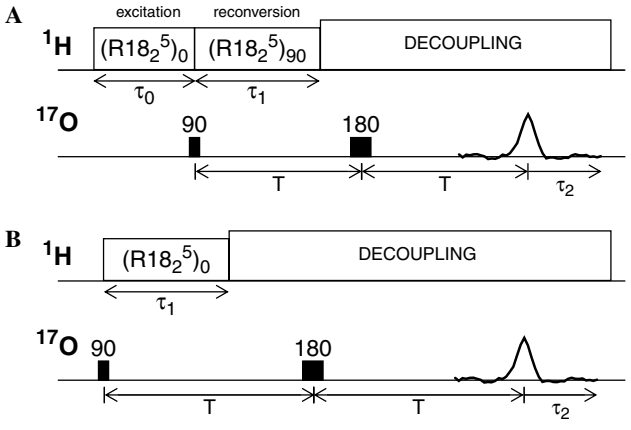

Fig. 1. (A) PRESTO-II pulse sequence. Recoupling periods are denoted by $R18_2^5$, where 18, 2, and 5 denote the symmetry numbers N, n, and v of the recoupling sequence. The subscript to the recoupling period denotes the overall rf phase in degrees. The ^{17}O flip angles correspond to rotations in degrees of the central transition and the echo intervals T correspond to a fixed integer number of rotor periods $\tau_r = 2\pi/\omega_r$. (B) Sequence for generating a dipolar oscillation for a 1Q coherence.

This sequence of events leads to $^{1}H \rightarrow {}^{17}O$ polarization transfer. The principles of PRESTO-II have been explained in detail for spin-1/2 systems in [27] and will not be repeated here. The pulse sequence works in the same way for the ^{17}O central transition as for spin-1/2 nuclei, since the large second-order quadrupolar shift is exactly refocused by the rotor-synchronized Hahn echo. In principle, there could be additional effects due to higher-order coupling terms, such as the cross-term between the ^{17}O quadrupolar interaction and the ^{1}H–^{17}O heteronuclear coupling. However, numerical simulations indicate that the effect of these higher-order terms is negligible in practice (see below).

The PRESTO-II sequence may be used for generating QD correlation spectra by holding τ_0 and T fixed, while incrementing τ_1. Double Fourier transformation with respect to the dipolar evolution interval τ_1 and the signal acquisition time coordinate leads to 2D QD correlation spectra, as shown in Fig. 2 below.

The heteronuclear dipolar oscillations may also be investigated without $^{1}H \rightarrow {}^{17}O$ polarization transfer by the pulse sequence in Fig. 1B. In this case, central-transition ^{17}O transverse magnetization is generated directly by a 90° pulse, and allowed to evolve in the presence of a $R18_2^5$ sequence applied to the ^{1}H nuclei for an interval τ_1. The ^{17}O chemical shifts and second-order quadrupolar shifts are refocused by a rotor-synchronized Hahn echo with a fixed interpulse interval T. TPPM decoupling is again used to suppress the heteronuclear interactions during the echo intervals. A QD correlation spectrum is generated by incrementing the dipolar evolution interval τ_1 while holding the interpulse interval T fixed, followed by a two-dimensional Fourier transform of the data matrix. If desired, enhanced central-transition ^{17}O magnetization may be generated by manipulating the ^{17}O satellite transition populations prior to the 90° pulse, by applying suitably modulated rf fields [29–33]. If this is done, the pulse sequence in Fig. 1B often generates comparable or higher signal strength per unit time than the PRESTO method, especially since the ^{17}O longitudinal relaxation time is often shorter than that of the protons. However, the PRESTO technique in Fig. 1A does allow suppression of the ^{17}O signal from non-protonated sites, which is often useful.

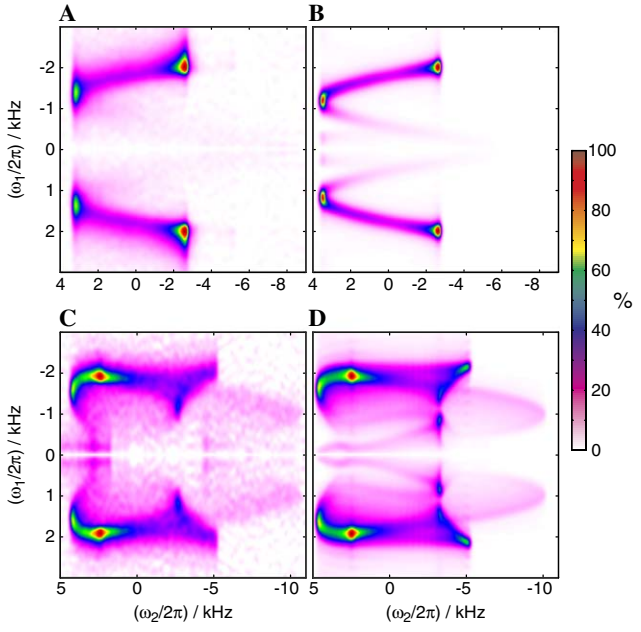

Fig. 2. (A) Experimental and (B) simulated QD correlation spectra for $Mg(^{17}OH)_2$ and (C and D) similarly for [U-^{13}C,^{17}O]glycine · HCl. The horizontal (quadrupolar) and vertical (dipolar) axes correspond to Fourier transforms with respect to intervals τ_2 and τ_1, respectively. All data were taken at 16 kHz MAS in a field of 9.4 T, using $R18_2^5$, $\tau_0 = 125.1$ μs, $\tau_1 = 69.4$ μs and $T = 3.73$ ms. The asymmetrical cross section in the indirect dimension is thought to be due to rf inhomogeneity as described in the text.

3. Experimental

3.1. Samples

The ^{1}H–^{17}O recoupling methods were tested on two different ^{17}O-labelled samples.

$Mg(^{17}OH)_2$ was synthesized by slowly adding 35–40% ^{17}O-enriched H_2O (Cambridge Isotope Laboratories) to a suspension of Mg_3N_2 (99.5+%, 325 mesh, Sigma–Aldrich) in CCl_4, while stirring vigorously for 12 h. The resulting grey lumps of $Mg(^{17}OH)_2$ were dried under high vacuum. Wide-angle powder X-ray diffraction was used to confirm the correctness and purity of the crystal phase [34].

[U-^{13}C,^{17}O]glycine · HCl was synthesized following the procedure described in [35]. The ^{17}O enrichment was approximately 35%. The ^{13}C nuclei were introduced for purposes unrelated to this study. [U-^{13}C,^{17}O]glycine · HCl has two different ^{17}O sites, one protonated, and one unprotonated. Both sites lack local symmetry.

3.2. NMR experiments

NMR experiments at 9.4 T were performed on a Varian InfinityPlus system, whilst experiments at 14.1 T were performed on a Chemagnetics Infinity console, using standard 2.5, 3.2 and 4 mm T3 double- and triple-resonance probeheads tuned to ^{1}H and ^{17}O. All experiments were run at 16 kHz MAS and at room temperature. Typical 90° pulse lengths for the ^{17}O central transition were 5 μs. The $R18_2^5$ recoupling sequences used a nominal ^{1}H nutation frequency of 72 kHz. Proton decoupling was implemented using TPPM modulated ^{1}H irradiation [28] using a rf field strength corresponding to a 100 kHz nutation frequency. The use of TPPM decoupling rather than CW decoupling was critical to the success of these experiments, since the TPPM modulation greatly reduces the decay of the signal during the long echo intervals [36]. The pronounced differential decay across the second-order quadrupolar pattern, which was prominent when using continuous-wave (CW) decoupling, was thus greatly reduced.

The 2D QD experiment on $Mg(^{17}OH)_2$ was performed using 384 transients for every increment of τ_1, a 2 s recycle delay and a 60 rotor-period echo ($T = 3.73$ ms). The first recoupling interval was fixed at $\tau_0 = 125.1$ μs, while τ_1 was incremented in steps of 5 pairs of R elements (69.4 μs), using 54 increments in total. For [^{13}C,^{17}O]glycine · HCl there were 2048 transients for each increment of τ_1, and a 1 s recycle delay. Dummy scans were taken to obtain a steady-state before the start of each 2D experiment.

For the 1D experiments using $Mg(^{17}OH)_2$ 32 transients were recorded with $\tau_0 = \tau_1 = 125.1$ μs, and an echo interval $T = 125.1$ μs. A longer recycle delay of 20 s was used between transients to ensure full thermal equilibrium. For [^{13}C,^{17}O]glycine · HCl, 256 transients were taken with $\tau_0 = \tau_1 = 125.1$ μs and a 6 s recycle delay, whilst at 14.1 T, 32 transients were taken with $\tau_0 = \tau_1 = 139.0$ μs, echo interval $T = 250.2$ μs, and a 10 s recycle delay.

3.3. Data processing

The PRESTO-II pulse sequence in Fig. 1A yields a dipolar oscillation which is sine-modulated with respect to the variable delay τ_1. To obtain pure absorption two-dimensional QD spectra, a 90° phase shift was applied after the standard cosine Fourier transform, followed by an inversion of one half of the spectrum in the indirect dimension. This is equivalent to a sine Fourier transform in the indirect dimension. All spectra were processed using the matNMR processing package [37].

3.4. Numerical simulations

Piece-wise constant rotating-frame density matrix simulations were performed using GAMMA [38] and included all pulses, timings and field strengths as executed in the experiments. A discrete time resolution of 434 ns was used (144 steps per rotor cycle). Phase transients, rf inhomogeneity and relaxation were not generally included, except for a few more extensive simulations. Powder averaging was done following the procedure by Cheng [39], with 50000 orientations used for the 2D simulations. All calculations used truncated Hamiltonians, which included the second-order quadrupolar interaction and the second-order quadrupole–dipole–dipole cross-term [40], whose magnitude was significant in the studied systems. J couplings were not included in the calculations since DFT calculations have shown them to be insignificant for glycine · HCl and no J coupling could be detected experimentally [41].

Simulations including phase transients, modelled as described in [42], used a discrete time resolution of 14.4 ns.

Laboratory-frame spin simulations were also performed for a selection of single molecular orientations in order to validate the second-order perturbation theory for the heteronuclear case [40]. These simulations included the untruncated forms of all spin interactions and a time-dependent rf Hamiltonian and used a discrete time resolution of 10 ps.

4. Results

4.1. Quadrupole–dipole correlation spectra

Fig. 2 shows two-dimensional QD spectra obtained for two ^{17}O-labelled materials, $Mg(^{17}OH)_2$ and [U-^{13}C,^{17}O]glycine · HCl, and the corresponding simulations. Both experimental spectra were obtained using the PRESTO-II pulse sequence shown in Fig. 1A.The total measuring time for the $Mg(^{17}OH)_2$ spectrum in Fig. 2A was 11.5 h and that for [U-^{13}C,^{17}O]glycine · HCl in Fig. 2C was 30 h.

4.2. $Mg(^{17}OH)_2$

In $Mg(^{17}OH)_2$ the 3-fold crystal symmetry [43] dictates coaxial quadrupolar and dipolar interaction tensors, leading to QD spectra with the simple form shown in Fig. 2A. The simulation shown in Fig. 2B agrees well with the experimental data, with the ^{1}H–^{17}O dipole–dipole coupling estimated to be 13.3 ± 0.3 kHz. This value is smaller than expected, as is discussed below. The simulation for $Mg(^{17}OH)_2$ shown in Fig. 2B used a ^{1}H–^{17}O dipole–dipole coupling constant $b/2\pi = 13.3$ kHz, with coaxial ^{1}H CSA, ^{17}O quadrupole coupling and dipolar tensors. The quadrupole parameters were $C_Q = 6.835$ MHz and $\eta = 0.0$, as determined from 1D spectra taken under static and MAS conditions (not shown). These values correspond well with previously reported values [10,44]. No isotropic shift was included. Values for the ^{1}H CSA were taken from [45].

The experimental dipolar oscillations for $Mg(^{17}OH)_2$, measured at a field of 9.4 T, are shown at the positions of the two second-order quadrupolar lineshape singularities in Fig. 3B. This shows the very high definition of the heteronuclear splitting, and the difference in the splitting magnitude at the two main singularities of the ^{17}O second-order powder pattern. Fig. 3C shows the experimental heteronuclear dipolar oscillations for $Mg(^{17}OH)_2$, obtained using the pulse sequence in Fig. 1B, at a field of 9.4 T. The definition of the dipolar oscillations is again very high, with the same dipolar oscillation frequencies as in Fig. 3B, as can be seen from the Fourier-transformed spectra in Figs. 3E and F. The couplings typically vary across the quadrupolar pattern, which reflects the relative orientation of the quadrupolar and dipolar tensors.

Fig. 4B shows the experimental dipolar oscillations for $Mg(^{17}OH)_2$, measured at a field of 14.1 T, using the pulse sequence in Fig. 1B. The heteronuclear dipolar splitting is again well defined, with a frequency that is indistinguishable from the result obtained at lower magnetic field.

4.3. [U-^{13}C,^{17}O]glycine · HCl

The QD spectrum of [U-^{13}C,^{17}O]glycine · HCl is shown in Fig. 2B and has a complex form, reflecting the fact that the interaction tensors are not coaxial. The simulation shown in Fig. 2D fits the data well. This simulation was obtained using a heteronuclear coupling of

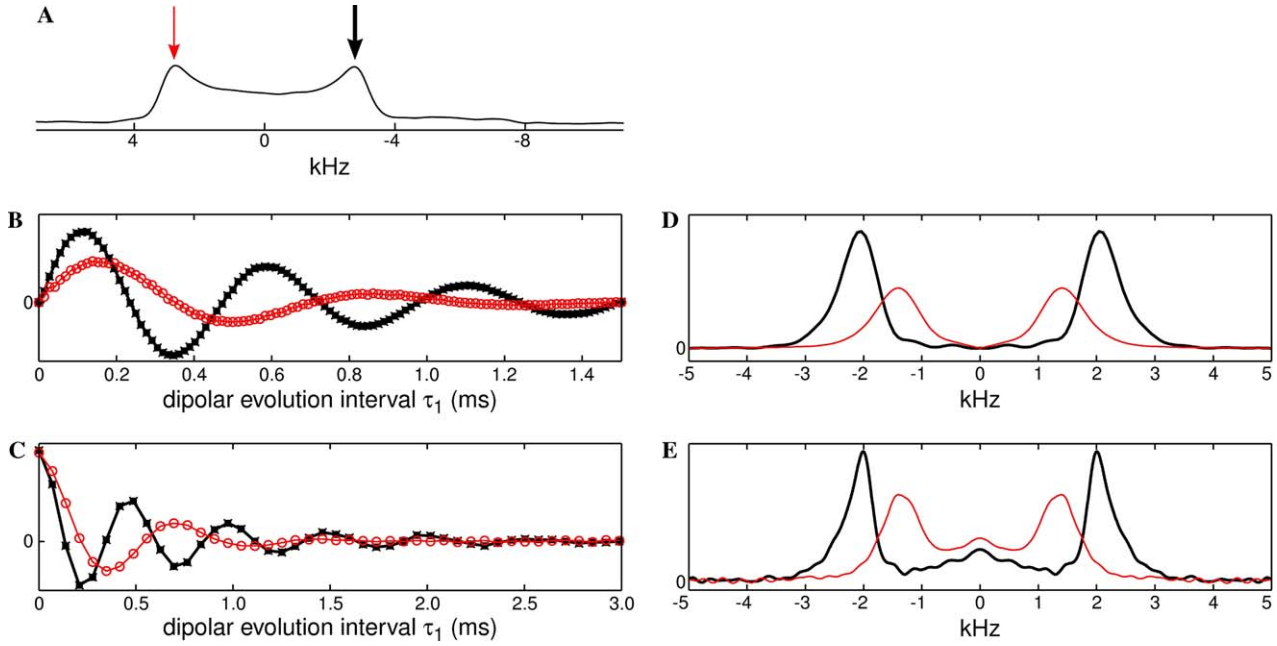

Fig. 3. (A) Central transition lineshape of $Mg(^{17}OH)_2$ at 9.4 T with 16 kHz MAS. The arrows denote the left-hand and right-hand singularities. (B and C) Experimental dipolar oscillations obtained for $Mg(^{17}OH)_2$, using the pulse sequences of (B) Fig. 1A and (C) Fig. 1B. (D and E) The corresponding spectra after Fourier transformation. The red open circles with thin lines and the filled black squares with thick lines correspond to the left-hand and right-hand singularities of the second-order quadrupolar pattern, respectively. The two curves within each plot have the same absolute vertical scale. The asymmetrical cross section in the dipolar dimension is attributed to rf inhomogeneity, as described in the text.

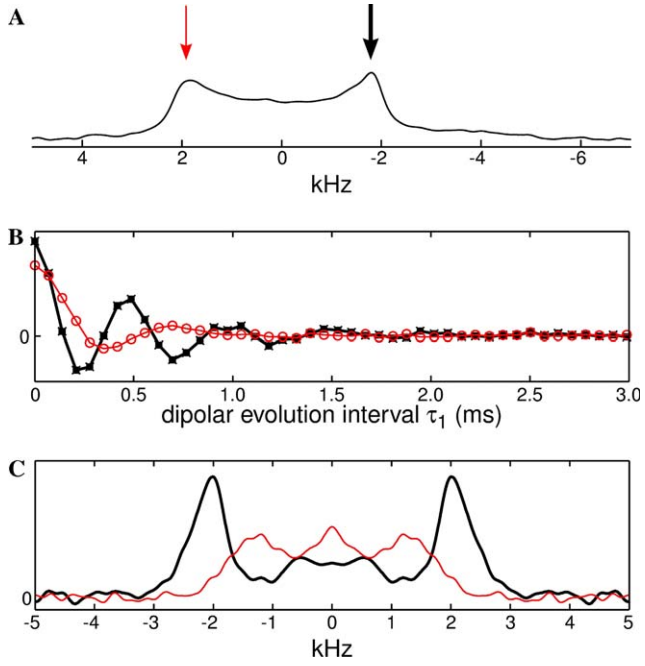

Fig. 4. (A) Central transition lineshape of lineshape of $Mg(^{17}OH)_2$ at 14.1 T with 16 kHz MAS. The arrows denote the left-hand and right-hand singularities. (B) Experimental dipolar oscillations obtained for $Mg(^{17}OH)_2$, using the pulse sequence of Fig. 1B. The red open circles with thin lines and the filled black squares with thick lines correspond to the left-hand and right-hand singularities of the second-order quadrupolar pattern, respectively. The two curves have the same absolute vertical scale. The asymmetrical cross section in the dipolar dimension is attributed to rf inhomogeneity, as described in the text.

12.6 ± 0.3 kHz, a value which is again surprisingly small, as discussed below.

The long calculation time of each simulation prevented global optimization of the interactions over the full parameter space. To obtain the final simulations the following procedure was used: (i) Preliminary three-spin simulations showed that the dipolar interactions between the ^1H and ^{17}O nuclei and the nearest ^{13}C nucleus only have a small effect on the simulated spectra. The simulations were therefore performed omitting the ^{13}C nuclei. (ii) It was found by simulation that the 9.4 T spectra are virtually unaffected by the magnitude and the orientation of the proton CSA, which was therefore ignored for the spectra at 9.4 T. (iii) The 9.4 T data were fitted by adjusting the ^{17}O quadrupole coupling parameters, starting from the values reported in [35]. A good match with the experimental result was obtained using ^{17}O quadrupole coupling parameters of $C_Q = 7.75$ MHz and $\eta = 0.19$, and Euler angles $(0°, 41°, 86°) \pm 5°$ relating the principal axis system of the ^1H–^{17}O dipole coupling tensor to that of the quadrupole coupling tensor, following the convention of [46]. The sensitivity of the QD spectra to the relative orientation of the quadrupole and dipole tensors is shown in Fig. 5. (iv) The final fits were performed by incorporating ^{17}O CSA principal values and principal axis orientations estimated by DFT calculations following the scheme described in [47]. The principal values of the ^{17}O chemical shift anisotropy tensor were $(\delta_{11}, \delta_{22}, \delta_{33}) = (343, 107, 84)$ ppm (deshielding

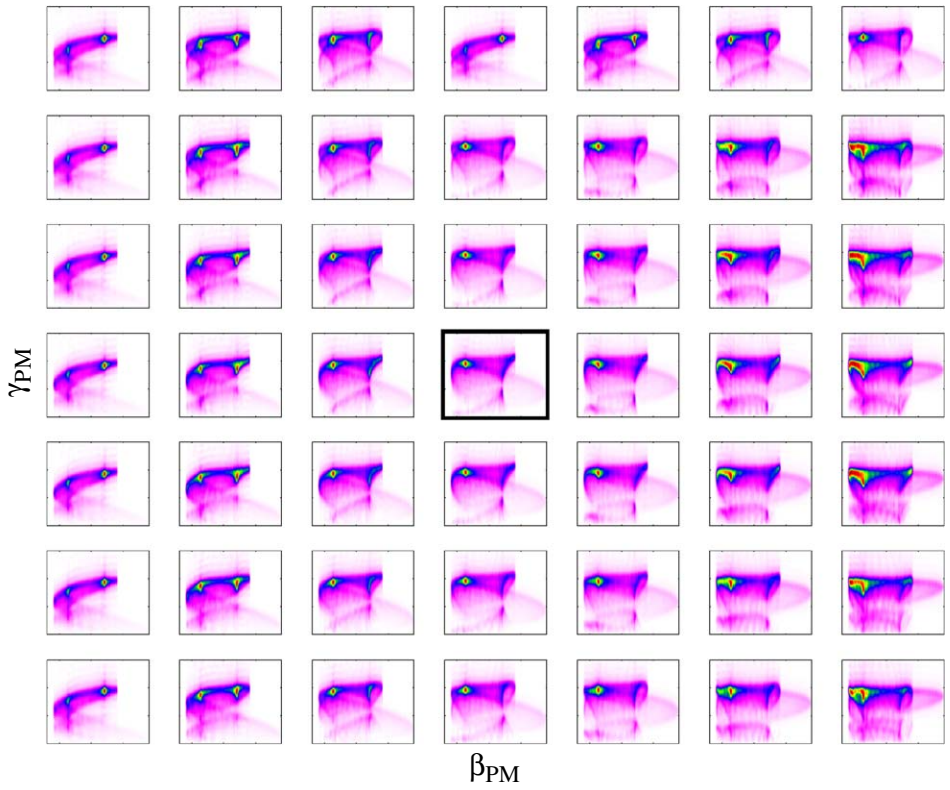

Fig. 5. Simulated QD spectra for [U-^{13}C,^{17}O]glycine · HCl at 9.4 T (top-half only) to indicate the sensitivity towards the relative orientation of the quadrupolar and dipolar tensors. The highlighted spectrum used Euler angles (0°, 41°, 86°) to relate the principal axis system of the dipolar to the quadrupolar tensor. The angles are incremented by 10° between spectra. Note that larger deviations in spectral shape are found outside the shown region.

shifts relative to water at 0 ppm), and the principal axis system of the CSA tensor was related to that of the quadrupole coupling tensor by the Euler angles (−273°, −105°, −82°).

The heteronuclear coupling, the relative orientation of the quadrupole and the dipole tensors and the quadrupole parameters all give rise to uncorrelated spectral changes, allowing these parameters to be optimized independently and sequentially.

For materials with large proton CSA interactions a strong influence of the proton can be detected at high magnetic fields. Fig. 6 shows the changes in simulated QD spectra at 14.1 T, using the above-mentioned parameters for glycine. A tensor anisotropy of 18.2 ppm and an asymmetry of 0.03 were assumed for the calculations, in agreement with values obtained by ab initio calculations. The simulation in the center of Fig. 6 indicates the best fit with a QD spectrum taken at 14.1 T (not shown here) and used Euler angles (0°, 5°, and 5°).

Finally, it was found a posteriori that the match between simulations and experimental results obtained at 9.4 T could be improved by allowing for a slight offset of the spinning axis from the magic angle by −0.5°. Simulations have demonstrated that such an offset only affects the second-order quadrupole dimension and not the dipolar dimension (not shown).

4.4. $^{1}H \rightarrow {}^{17}O$ polarization transfer

The PRESTO-II sequence of Fig. 1A involves polarization transfer from ^{1}H nuclei to the ^{17}O central transition. This can, in principle, lead to considerable ^{17}O signal enhancement, since ^{1}H nuclei have a larger magnetic moment than ^{17}O nuclei. In a powder, the maximum theoretical enhancement, compared to direct excitation of the ^{17}O central transition, is $0.73 \times \gamma(^{1}H)/\gamma(^{17}O) = 5.38$, where the factor of 0.73 arises from the geometric dependence of the recoupling, in the case of pulse sequences displaying "γ-encoding" [48]. Unfortunately, this large potential enhancement proved to be difficult to obtain in practice.

Figs. 7A and B compares PRESTO with a simple Hahn-echo scheme for two different magnetic fields, using a powder sample of $Mg(^{17}OH)_2$. Both 9.4 T spectra in Fig. 7A resulted from the accumulation of 128 transients, for the 14.1 T spectra in Fig. 5B 32 transients were accumulated, with other parameters being the same. An enhancement by a factor of around 2 was achieved for PRESTO in a magnetic field of 9.4 T, but the enhancement was less at 14.1 T. The loss is attributed to the effect of relaxation during the recoupling and spin echo intervals, and to the interference of the recoupled ^{1}H CSA, which becomes more prominent at high magnetic field.

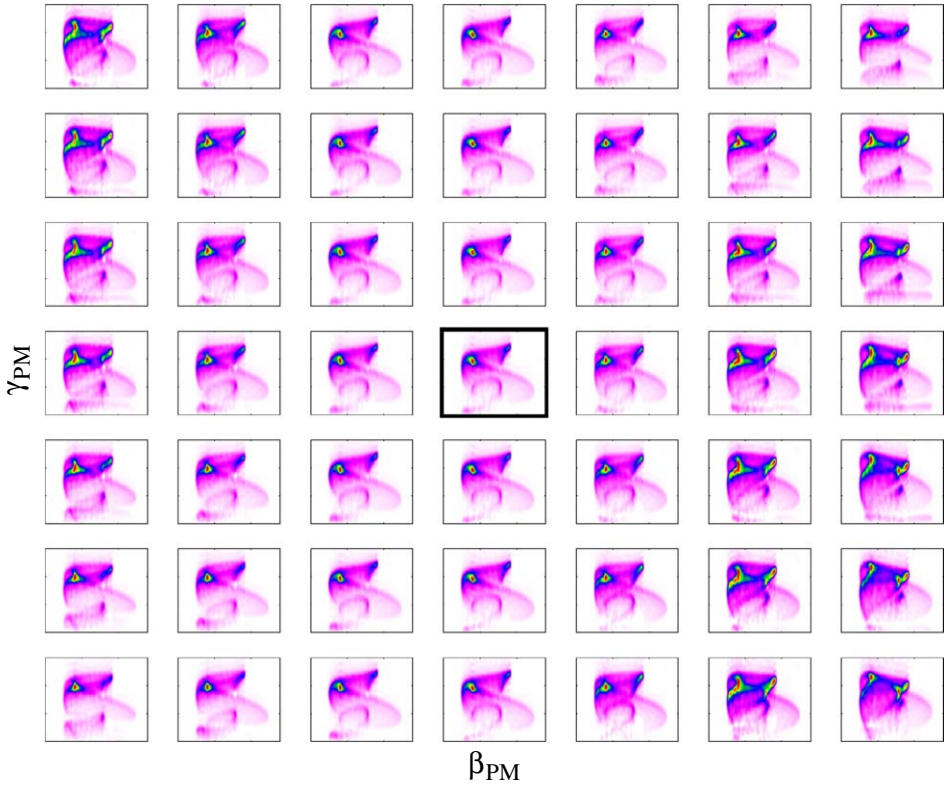

Fig. 6. Simulated QD spectra for [U-^{13}C,^{17}O]glycine · HCl at 14.1 T to indicate the sensitivity towards the relative orientation of the quadrupolar and proton CSA tensors. The highlighted spectrum used Euler angles (0°, 5°, and 5°) to relate the principal axis system of the CSA to the quadrupolar tensor. The angle α_{PM} was not varied because CSA tensor was near-symmetric. The angles are incremented by 10° between spectra.

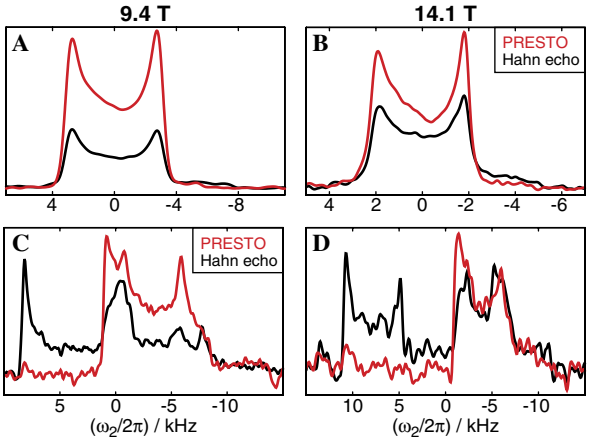

Fig. 7. (A and B) Solid-state ^{17}O NMR spectra of Mg(^{17}OH)2 obtained using either a Hahn echo (black) or PRESTO (red) at magnetic fields of 9.4 T and 14.1 T. (C and D) Data for [U-^{13}C,^{17}O]glycine · HCl under similar conditions. All data were taken at a spinning speed of 16 kHz. All PRESTO experiments used $\tau_0 = \tau_1 = 125.1$ μs and $T = 125.1$ μs, except (D), where $\tau_0 = \tau_1 = 139.0$ μs and T = 250.2 μs was used.

To allow a quantitative comparison of the PRESTO and direct-excitation methods long recycle delay (20 s) was used between transients to ensure full thermal equilibrium. However, the ^{17}O nuclei actually have a shorter spin–lattice relaxation time than the ^{1}H nuclei, so the comparison would be less favourable for PRESTO, if optimal relaxation conditions were used in both cases. Furthermore, the directly excited ^{17}O signal could be readily enhanced by a factor of 2 or more by manipulating the ^{17}O satellite populations [29–33]. We conclude that $^{1}H \rightarrow {}^{17}O$ PRESTO transfer is unlikely to become a competitive method for ^{17}O signal enhancement.

4.5. ^{17}O spectral editing

Although signal enhancement by $^{1}H^{17}O$ PRESTO transfer may not be advantageous, polarization transfer from the ^{1}H nuclei does lead to useful spectral editing capabilities. This is illustrated by the ^{17}O spectra of [U-^{13}C,^{17}O]glycine · HCl shown in Figs. 7C and D. Spectra at both magnetic fields show the suppression of signals from the non-protonated ^{17}O site. The selectivity is more easily visible at the higher magnetic field, where the two broad lineshapes are resolved in the Hahn echo spectrum. Note that PRESTO editing is complementary to approaches that suppress the ^{17}O signals of protonated sites, such as interruption of the proton decoupler field during a spin echo interval [49].

5. Discussion

The experimental results show that it is possible to achieve efficient symmetry-based recoupling of the hetero-

nuclear ^{1}H–^{17}O dipole–dipole interactions. Heteronuclear recoupling may be used to achieve ^{1}H–^{17}O polarization transfer, ^{17}O spectral editing, and to generate two-dimensional correlation spectra which are very sensitive to the relative orientations of the ^{1}H–^{17}O interaction tensor and the electric field gradient at the site of the ^{17}O nucleus. It has proved possible to simulate the form of these two-dimensional QD spectral lineshapes with high fidelity.

One of our initial aims was to enhance ^{17}O signals by polarization transfer from the more magnetic ^{1}H nuclei. This was only partially successful. Although polarization transfer was achieved, it proved difficult to achieve truly useful signal enhancements, especially since ^{1}H magnetization often equilibrates more slowly than ^{17}O magnetization. In most cases it will be easier to enhance central-transition ^{17}O signals by manipulation of the ^{17}O satellite populations [29–33]. Nevertheless, ^{1}H^{17}O polarization transfer is likely to be useful for the selective observation of ^{17}O signals from protonated oxygens.

The two-dimensional QD spectra clearly provide a great deal of information on the quadrupolar and dipolar coupling parameters, and their relative orientation. However, the observed heteronuclear splittings correspond to ^{1}H–^{17}O dipolar couplings that are much smaller than that expected on the basis of neutron diffraction coordinates. Consider, for example, the heteronuclear splitting in the single-quantum QD spectrum of Mg(^{17}OH)$_2$ (Figs. 2A, 3B and C, and 4B). A good match with simulation requires a heteronuclear coupling of 13.3 ± 0.3 kHz, which corresponds to a OH distance of $r_{OH} = 107 \pm 1$ pm, if all atomic motion is ignored. This value may be contrasted with the internuclear distance of $r_{OH} = 95$ pm, estimated by neutron diffraction of a natural crystal at room temperature [43]. If no motional correction is applied, the neutron distance corresponds to a dipolar coupling of 19.0 kHz. The observed dipolar coupling is therefore around 30% too low. This is a striking discrepancy.

Proton motion, and delocalization of the proton wavefunction, clearly account for part of the discrepancy. Single-crystal neutron diffraction has led to a detailed picture of the proton dynamics in Mg(OH)$_2$ [43,50,51]. At ambient temperatures, the protons move rapidly between three symmetry-related sites, situated just off the 3-fold axis [43]. In each of these sites, the O–H bond vector makes an angle of $\theta = 9°$ with respect to three-fold axis. Rapid exchange between these sites is expected to scale the OH dipolar coupling by a factor of $\frac{1}{2}(3\cos^2\theta - 1) = 0.96$. The anticipated value of the dipolar coupling constant, correcting for this 3-site motion, is therefore 18.3 kHz. The experimentally observed value is 27% smaller. Measurements performed at a temperature of approximately 150 K (uncalibrated) showed no differences in the dipolar splitting (not shown).

We have investigated the possibility that instrumental imperfections or spin dynamical effects could lead to a low estimate of the DD coupling. For example, it is possible to simulate the effect of limited probe response times, and phase transients in the transmitter channel, by the same simple mathematical model as used in [42]. We used $\lambda_{tran} = 3.2 \times 10^6\ s^{-1}$ and $\lambda_Q = 1.2 \times 10^6\ s^{-1}$ as defined in [42]. The $R18_2^5$ sequence is predicted to be compensated for these transient effects and this has been verified by numerical simulation. A deviation of less than 3% in the dipolar splitting was observed. Furthermore, these experiments were carried out on different models of spectrometer, using different probes and at different magnetic field strengths, all gave very similar results.

The effect of rf inhomogeneity has been examined by simulation. It was found that an rf field distribution always leads to an asymmetric broadening in the dipolar dimension of the QD spectra, with a tail stretching to high oscillation frequencies. This effect can easily be recognized in the experimental QD spectrum of Fig. 2A. Rf inhomogeneity cannot be responsible for the observed low values of the dipolar splitting.

In principle, ^{1}H CSA can influence the heteronuclear splittings generated by the $R18_2^5$ sequence, providing that the ^{1}H CSA and the ^{1}H–^{17}O dipole–dipole coupling do not share a common principal axis system. However, in the case of Mg(OH)$_2$, the principal axis systems coincide due to crystallographic symmetry, so the ^{1}H CSA has a negligible effect on the observed spectra. Indeed, numerical simulations using realistic values for the ^{1}H CSA ($\delta_{zz} - \delta_{iso} = 7.5$ ppm [45]) show no significant change in the heteronuclear splitting. Furthermore, we observe no significant dependence of the splitting on the static magnetic field, which also disfavours a CSA-based mechanism.

We have also investigated the possible effect of neighbouring protons by numerical simulation. The ^{1}H–^{1}H interactions are rather strong in brucite. Every proton has three ^{1}H neighbours, each at a distance of 198.6 pm [43]. Inclusion of the three nearest hydrogens for Mg(^{17}OH)$_2$ showed no change in dipolar frequency, only a stronger decay of the dipolar oscillation.

Since ^{17}O is a spin-5/2 nucleus with a considerable electric quadrupole moment, care is required in numerical simulations to take into account the partial breakdown of the high-field approximation. For example, it is well-known that the lineshapes of a spin-1/2 coupled to a quadrupolar nucleus are split by a second-order quadrupole-dipole cross term [40]. The dominant second-order broadening of the central transition peak is also a result of deviations from the high-field limit. Our numerical simulations include these second-order effects (including all known second-order cross terms with other interactions) by incorporating second-order correction terms in the secular spin Hamiltonian. It was found that all of these high-order terms have negligible influence on the heteronuclear oscillations.

In addition, we double-checked the perturbation theory of the spin dynamics by performing laboratory frame simulations of some selected orientations, using a discrete time resolution of 10 ps. In these numerically intensive simulations, the full forms of all spin interactions were used (including all non-secular terms), the static magnetic field

was included explicitly, and the rf fields were represented as time-dependent oscillating fields. Only small deviations (<4%) from the rotating-frame simulations were observed. The stated error margin of 0.3 kHz in the DD coupling, to the best of our current knowledge, takes into account all reasonable uncertainties in the instrumental and spin-interaction parameters.

It should be noted that van Eck and Smith [10] reported a much higher estimate of the ^{1}H–^{17}O dipole–dipole coupling in $Mg(^{17}OH)_2$ from a static experiment. Their reported dipolar coupling of 16.25 kHz is only 15% smaller than that estimated from the 95 pm neutron distance. However, it should be noted that the Lee-Goldburg method used by van Eck and Smith is notoriously difficult to calibrate, and that these authors do not report confidence limits. In contrast, the symmetry-based recoupling sequences used in our work have a robust scaling factor and were carefully calibrated by conducting ^{1}H–^{13}C recoupling experiments under identical conditions before the ^{17}O measurements.

The remaining discrepancy could be due to additional librational motion of the OH bond and spreading of the proton wavefunction, or a different, unidentified, mechanism, which was not detected in the neutron studies [43,50,51]. However, very large librational motions would be required to explain the effect. To put this into perspective, discrepancies of around 10% are frequently observed between solid-state NMR measurements of ^{13}C–^{1}H dipolar couplings in solids and dipolar coupling values calculated from neutron C–H distance estimates. Such discrepancies are readily explained by librational motional models [52]. The observed discrepancy in the ^{1}H–^{17}O coupling appears to be at least twice as large as this.

The spectra of [U-^{13}C,^{17}O]glycine · HCl display a similar deviation between the NMR and neutron estimates of the O–H internuclear distance. There is a good match between experiment and simulation for a dipolar coupling of 12.6 ± 0.3 kHz. The neutron estimate of the internuclear distance is $r_{OH} = 100$ pm [53], which corresponds to a dipolar coupling of 16.3 kHz. As in the case of $Mg(^{17}OH)_2$, there is a discrepancy of around 30% between these values. Reasonable models of atomic motion may readily account for about 10% of this discrepancy, but the remaining deviation has not been explained.

In the case of [U-^{13}C,^{17}O]glycine · HCl, we checked that inclusion of a ^{35}Cl spin or a second ^{17}O nucleus in the simulations did not introduce significant differences. As noted above, preliminary simulations of the 2D QD spectra for [U-^{13}C,^{17}O]glycine · HCl showed that the ^{13}C closest to the ^{17}O nucleus only has a minor effect on the shape of the spectrum.

A large *J*-anisotropy of around 3 kHz could potentially account for the surprisingly low DD coupling. Although a *J*-anisotropy of this magnitude seems unlikely, this mechanism cannot be ruled out without performing detailed quantum calculations.

The small dipolar splitting could also be due to an unidentified motional process, possibly involved in a complex interference with the heteronuclear recoupling. We are planning more detailed temperature-dependent studies, which hopefully will shed some light on this hypothesis.

We have also observed heteronuclear splittings of the ^{17}O multiple-quantum coherences by performing symmetry-based proton recoupling during the evolution period of a MQ-MAS experiment [11,12]. We will report this data in a separate publication.

6. Conclusion

In conclusion, we have showed that symmetry-based recoupling is an effective tool for the NMR study of ^{17}O-^{1}H spin pairs in the solid state. Two-dimensional QD correlation spectroscopy allows detailed investigation of dipole–dipole couplings and relative tensor orientations, providing a wealth of detailed electronic and molecular structural information. The method is applicable to half-integer quadrupolar nuclei with large dipolar couplings to a spin species, even if there are strong couplings between the spin species, under fast MAS. This is difficult to achieve using existing methods. Weak heteronuclear couplings are currently not within the scope of the method and REDOR-derived sequences [18–22] may be preferable in such cases.

The magnitudes of the observed heteronuclear splittings are much smaller than those expected from neutron estimates of the internuclear distances. The discrepancies appear to be too large to attributed to wavefunction delocalization, librational motion, or *J*-anisotropy, and are unexplained at the time of writing.

Acknowledgments

We acknowledge financial support from Marie Curie, fellowship HPMF-CT-2002-01917, and EPSRC (UK). Xin Zhao is acknowledged for initial input, Ole Johannessen and Andrew Howes for technical support and Andreas Kukol for enriching the glycine sample. We also thank Clare Grey and Andreas Brinkmann for discussions.

References

[1] L.M. Bull, A.K. Cheetham, A. Samoson, T. Anupõld, A. Reinhold, J. Sauer, B. Bussemer, V. Moravetski, Y. Lee, S. Gann, J. Shore, A. Pines, R. Dupree, A high-resolution 17O NMR study of siliceous zeolite faujasite, J. Am. Chem. Soc. 120 (1998) 3510–3511.

[2] L.M. Bull, B. Bussemer, T. Anupõld, A. Reinhold, A. Samoson, J. Sauer, A.K. Cheetham, R. Dupree, A high-resolution O-17 and Si-29 nmr study of zeolite siliceous ferrierite and ab initio calculations of NMR parameters, J. Am. Chem. Soc. 122 (2000) 4948–4958.

[3] L. Peng, Y. Liu, N. Kim, J.E. Readman, C.P. Grey, Detection of Brønsted acid sites in zeolite HY with high-field ^{17}O-MAS-NMR techniques, Nat. Mater. 4 (2005) 216–219.

[4] I. Farnan, P.J. Grandinetti, J.H. Baltisberger, J.F. Stebbins, U. Werner, M.A. Eastman, A. Pines, Quantification of the disorder in network-modified silicate glasses, Nature 358 (1992) 31–35.
[5] N. Kim, C.P. Grey, Probing oxygen motion in disordered anionic conductors with 17O and 51V MAS NMR spectroscopy, Science 297 (2002) 1317–1320.
[6] V. Lemaitre, R.R. Planque, A.P. Howes, M.E. Smith, R. Dupree, A. Watts, New insights into the bonding arrangements of L- and D-glutamates from solid state ^{17}O NMR, J. Am. Chem. Soc. 126 (2004) 15320–15321.
[7] T. Steiner, The hydrogen bond in the solid state, Angew. Chem. Int. Ed. 41 (2002) 48–76.
[8] G.A. Jeffrey, Hydrogen Bonding in Biological Structures, Springer, Berlin, 1991.
[9] D. Freude, J. Haase (Eds.), NMR, Basic Principles and Progress, vol. 29, Springer Verlag, Berlin, 1993, pp. 1–90, Ch. Quadrupole effects in solid-state NMR.
[10] E.R.H. van Eck, M.E. Smith, Orientation of the quadrupole and dipole tensors of hydroxyl groups by ^{17}O quadrupole separated local field NMR, J. Chem. Phys. 108 (1998) 5904–5912.
[11] L. Frydman, J.S. Harwood, Isotropic spectra of half-integer quadrupolar spins from bidimensional magic-angle spinning NMR, J. Am. Chem. Soc. 117 (1995) 5367–5368.
[12] A. Medek, J.S. Harwood, L. Frydman, Multiple-quantum magic-angle spinning NMR: a new method for the study of quadrupolar nuclei in solids, J. Am. Chem. Soc. 117 (1995) 12779–12787.
[13] Z. Gan, Isotropic NMR spectra of half-integer quadrupolar nuclei using satellite transitions and magic angle spinning, J. Am. Chem. Soc. 122 (2000) 3242.
[14] Z. Gan, Satellite transition magic angle spinning nuclear magnetic resonance spectroscopy of half-integer quadrupolar nuclei, J. Chem. Phys. 114 (2001) 10845.
[15] A.J. Vega, CP/MAS of quadrupolar S=3/2 nuclei, Solid State NMR 1 (1992) 17–32.
[16] A.J. Vega, MAS NMR spin locking of half-integer quadrupolar nuclei, J. Magn. Res. 96 (1992) 50.
[17] W. Sun, J.T. Stephen, L.D. Potter, Y. Wu, Rotation-induced resonance and second-order quadrupolar effects on spin locking of half-integer quadrupolar nuclei, J. Magn. Res. A 116 (1995) 181–188.
[18] T. Gullion, J. Schaefer, Rotational-echo double-resonance NMR, J. Magn. Res. 81 (1989) 196–200.
[19] C.A. Fyfe, K.T. Mueller, H. Grondey, K.C. Wong-Moon, Dipolar dephasing between quadrupolar and spin-1/2 nuclei. REDOR and TEDOR NMR experiments on VPI-5, Chem. Phys. Lett. 199 (1992) 198–204.
[20] T. Gullion, Detecting C-13-O-17 dipolar interactions by rotational-echo, adiabatic-passage, double-resonance NMR, J. Magn. Res. A 117 (1995) 326–329.
[21] A. Goldbourt, S. Vega, T. Gullion, A.J. Vega, Interatomic distance measurements in solid-state NMR between a spin-1/2 and a spin-5/2 using a universal REAPDOR curve, J. Am. Chem. Soc. 125 (2003) 11194–11195.
[22] C. Fernandez, D.P. Lang, J.P. Amoureux, M. Pruski, Measurement of heteronuclear dipolar interactions between quadrupolar and spin-1/2 nuclei in solids by multiple-quantum REDOR NMR, J. Am. Chem. Soc. 120 (1998) 2672–2673.
[23] A.W. Hing, S. Vega, J. Schaefer, Transferred-echo double-resonance NMR, J. Magn. Res. 96 (1992) 205–209.
[24] M. Edén, M.H. Levitt, Pulse sequence symmetries in the nuclear magnetic resonance of spinning solids: application to heteronuclear decoupling, J. Chem. Phys. 111 (1999) 1511–1519.
[25] A. Brinkmann, M.H. Levitt, Symmetry principles in the nuclear magnetic resonance of spinning solids: heteronuclear recoupling by generalized Hartmann–Hahn sequences, J. Chem. Phys. 115 (2001) 357–384.
[26] M.H. Levitt, Symmetry-based pulse sequences in magic-angle spinning solid-state NMR, Encyc. NMR 9 (2002) 165–196.
[27] X. Zhao, W. Hoffbauer, J. Schmedt auf der Günne, M.H. Levitt, Heteronuclear polarization transfer by symmetry-based recoupling sequences in solid-state NMR, Solid State NMR 26 (2004) 57–64.
[28] A.E. Bennett, C.M. Rienstra, M. Auger, K.V. Lakshmi, R.G. Griffin, Heteronuclear decoupling in rotating solids, J. Chem. Phys. 103 (1995) 6951–6958.
[29] A.P.M. Kentgens, R. Verhagen, Advantages of double frequency sweeps in static, MAS and MQMAS NMR of spin I=3/2 nuclei, Chem. Phys. Lett. 300 (1999) 435–443.
[30] Z. Yao, H.T. Kwak, D. Sakellariou, L. Emsley, P.J. Grandinetti, Sensitivity enhancement of the central transition signal of quadrupolar nuclei under magic-angle spinning, Chem. Phys. Lett. 327 (2000) 85–90.
[31] H.T. Kwak, S. Prasad, T. Clark, P.J. Grandinetti, Enhancing sensitivity of quadrupolar nuclei in solid-state NMR with multiple rotor assisted population transfers, Solid State NMR 24 (2003) 71–77.
[32] P.K. Madhu, K.J. Pike, R. Dupree, M.H. Levitt, M.E. Smith, Modulation-aided signal enhancement in the magic-angle spinning NMR of spin-5/2 nuclei, Chem. Phys. Lett. 367 (2003) 150–156.
[33] R. Siegel, T.T. Nakashima, R.E. Wasylichen, Signal enhancement of NMR spectra of half-integer quadrupolar nuclei in solids using hyperbolic secant pulses, Chem. Phys. Lett. 388 (2004) 441–445.
[34] R. Cerny, V. Valvoda, M. Chladek, Empirical texture corrections for asymmetric diffraction and inclined textures, J. Appl. Crystallogr. 28 (1995) 247–253.
[35] K.J. Pike, V. Lemaitre, A. Kubol, T. Anupõld, A. Samoson, A.P. Howes, A. Watts, M.E. Smith, R. Dupree, Solid-state ^{17}O NMR of amino acids, J. Phys. Chem. B 108 (2004) 9256–9263.
[36] G. De Paëpe, N. Giraud, P. Hodgkinson, A. Böckmann, L. Emsley, Transverse dephasing optimized solid-state NMR spectroscopy, J. Am. Chem. Soc. 125 (2003) 13938–13939.
[37] matNMR is a toolbox for processing NMR/EPR data in Matlab and can be downloaded freely at http://matNMR.sourceforge.net.
[38] S. Smith, T. Levante, B.H. Meier, R.R. Ernst, Computer simulations in magnetic resonance: an object oriented programming approach, J. Magn. Res. A 106 (1994) 75–105.
[39] V.B. Cheng, J.H.H. Suzakawa, M. Wolfsberg, Investigations of a nonrandom numerical method for multidimensional integration, J. Chem. Phys. 59 (1973) 3992–3999.
[40] M. Goldman, P.J. Grandinetti, A. Llor, Z. Olejniczak, J.R. Sachleben, J.W. Zwanziger, Theoretical aspects of high-order truncations in solid-state nuclear magnetic resonance, J. Chem. Phys. 97 (1992) 8947–8960.
[41] C. Gervais, R. Dupree, K.J. Pike, C. Bonhomme, M. Profeta, C.J. Pickard, F. Mauri, Combined first principles computational and experimental multinuclear solid-state NMR investigation of amino acids, J. Chem. Phys. A 109 (2005) 6960–6969.
[42] M. Carravetta, M. Edén, O.G. Johannessen, H. Luthman, P.J.E. Verdegem, J. Lugtenburg, A. Sebald, M.H. Levitt, Estimation of carbon–carbon bond lengths and medium-range internuclear distances by solid-state nuclear magnetic resonance, J. Am. Chem. Soc. 123 (2001) 10628–10638.
[43] L. Desgranges, G. Calvarin, G. Chevrier, Interlayer interactions in M(OH)2: a neutron diffraction study of Mg(OH)2, Acta Crystallogr. B 52 (1996) 82–86.
[44] T.H. Walter, G.L. Turner, E. Oldfield, Oxygen-17 cross-polarization NMR spectroscopy of inorganic solids, J. Magn. Res. 76 (1988) 106–120.
[45] R.E.J. Sears, R. Kaliaperumal, 1H shielding anisotropy in Mg(OH)2: the isolated OH-group, J. Chem. Phys. 88 (1988) 2284–2288.
[46] D.M. Brink, G.R. Satchler, Angular Momentum, third ed., Clarendon Press, Oxford, 1993.
[47] J.R. Yates, C.J. Pickard, M.C. Payne, R. Dupree, Theoretical investigation of oxygen-17 NMR shielding and electric field gradients in glutamic acid polymorphs, J. Phys. Chem. A 108 (2004) 6032–6036.
[48] N.C. Nielsen, H. Bildsøe, H.J. Jakobsen, M.H. Levitt, Double-quantum homonuclear rotary resonance: efficient dipolar recovery in

magic-angle spinning nuclear magnetic resonance, J. Chem. Phys. 101 (1994) 1805–1812.
[49] J.N. Shoolery, Some quantitative applications of C-13 NMR, Prog. NMR Spectrosc. 11 (1977) 79–93.
[50] W.R. Busing, H.A. Levy, Neutron diffraction study of calcium hydroxide, J. Chem. Phys. 26 (1957) 563–568.
[51] B.C. Chakoumakos, C.K. Loong, A.J. Schultz, Low-temperature structure and dynamics of brucite, J. Phys. Chem. B 101 (1997) 9458–9462.
[52] Y. Ishii, T. Terao, Theory and simulation of vibrational effects on structural measurements by solid-state nuclear magnetic resonance, J. Chem. Phys. 107 (1997) 2760–2774.
[53] A.R. Al-Karaghouli, F.E. Cole, M.S. Lehmann, C.R. Miskell, J.J. Verbist, T.F. Koetzle, Precision neutron diffraction structure determination of protein and nucleic acid components. xvii. Molecular and crystal structure of the amino acid glycine hydrochloride, J. Chem. Phys. 63 (1975) 1360–1366.